11th Australasian Fluid Mechanics Conference
University of Tasmania, Hobart, Australia
14-18 December 1992

FLOW CHARACTERISTICS IN AN S-SHAPED DIFFUSING DUCT WITH ASYMMETRIC INLET CONDITIONS

J.H. WHITELAW[1] and S.C.M. YU[2]

[1]Dept of Mechanical Engineering, Imperial College of Science, Technology & Medicine, London, UK

[2]School of Mechanical & Production Engineering, Nanyang Technological University, SINGAPORE

Abstract

Velocity and pressure characteristics of an S-shaped diffusing duct have been measured in a water tunnel with three asymmetric inlet conditions using laser-Doppler anemometry at a Reynolds number of 40,000. The three inlet conditions were introduced by thickening the boundary layer at various locations along the inlet circumference and corresponded to a side-slip, zero angle of attack (with effects of the fueslage) and low angle of attack if the S-shaped duct is considered as an intake passage for jet aircraft. The results are compared with those obtained with symmetrical inlet conditions of Rojas, Whitelaw and Yianneskis (1983) in the same diffuser and show that the location of the maximum velocity region approaching the inlet of the first bend determined the distribution of the secondary flow in the exit plane. In the first and the third cases, the exit flow had been modified to include an enlarged pair of contra-rotating vortices while these vortices are absent in the second case. The presence of the enlarged vortex pair had also impaired the non-uniformity of the corresponding streamwise mean velocity distribution at the exit. The maximum secondary flow velocity however, did not exceed 15% of the inlet bulk velocity in all cases investigated here.

1. Introduction

Considerable efforts have been expended to investigate the flow characteristics in S-shaped ducts of rectangular and circular cross-sections at different inlet conditions because of their applications in jet aircraft intake propulsion system, see for examples, Bradshaw and Bansod (1972), Anderson et al (1982), Rojas et al (1983) and more recently Whitelaw and Yu (1992). It is known that a pair of vortices rotating in the same sense as in the first bend, is formed at the outside wall of the second bend. The measurements of Anderson et al, involved mild curvature and thin inlet boundary layers and showed that the formation of the vortices was due to the changing sign of radial vorticity at the entrance of the second bend and the magnification of streamwise vorticity established in the first bend.The additional works of Rojas et al, with the same curvature, centre-line displacement of Anderson et al and a linear cross-sectional expansion, led to similar results. These investigations were essentially carried out with an uniform and symmetrical inlet profile both about the centre-line of the duct and the centre-plane of the cross-section. Inlet conditions to an intake may, however, be far from uniform and symmetric in flight and it is known, for example, from investigations such as that of Guo and Seddon (1983) that the consequences can be important, especially to the size and strength of the contra-rotating vortex pair. Despite their importance, relatively few detailed experimental information regarding asymmetric(or non-uniform) inlet conditions to an S-shaped duct had been published.

The present investigation is of two fold. First, to examine the consequences of non-uniform inlet conditions to an S-shaped diffuser and secondly, to provide detailed measurements of mean velocities, the corresponding turbulence levels, Reynolds shear stress and of the wall static pressure for the validation of CFD methods. The geometry of the S-diffuser chosen is identical to that of Rojas, Yianneskis and Whitleaw (1983) for which results with symmetrical inlet conditions are available for comparison.This paper deals with the experimental aspect of the investigation and a separate account of the related computation using the approach of Briley and McDonald (1984) can be found in Yu (1991).

Descriptions of the flow system, geometry of the S-diffuser and the laser-Doppler anemometer used to obtain the velocity measurements are described briefly in the following section. The results are presented and discussed in section 3. A list of the most important findings is given in section 4.

2. Flow Configurations, Instrumentations and Experimental Procedures

Figure 1 shows that the S-diffuser comprised two 22.5 degree bends of 280 mm mean radius of curvature made of transparent plexiglass and with the cross-section of the bends expanded linearly with downstream distance on both curved surfaces. The inlet cross-section was square (40 mm $\pm$ 0.1 x 40 $\pm$ 0.1 mm), and the exit cross-section after two 22.5 degrees of turning, was rectangular (40 $\pm$ 0.1 mm x 60 $\pm$ 0.1 mm) with an exit-to-inlet area ratio of 1.5. The ratio of the overall duct length to the centre-line displacement was 5.2. The streamwise distance (X_H) was measured along the centre-line in hydraulic diameters (D_H) of the upstream tangent from the inlet plane where the expansion began. Radial distance (R*) was measured from the outside wall of the first bend and from the inside wall of the second bend. The flow passed through a short upstream tangent of length 0.3 m (7.5 D_H) before the test section. The 0.5 mm trip wire of Rojas et al, located between the outlet of the contraction and the upstream tangent, i.e. at X_H= -7.5, was replaced by a 5 mm trip which extended from one side of the wall in three orientations corresponding to the three cases of figure 1(inset), that is: Case 1 : on the side of the outside wall of the first bend, case 2 : on the side of the inside wall of the first bend and case 3 : on the top side wall of the first bend. Measurements were obtained at a Reynolds number of 40,000 (associated Dean number 10,690) based on the hydraulic diameter of 40 mm, bulk velocity of 1.0 m/s at the upstream tangent and the physical properties of water at 20°C.

Measurements of the streamwise (U) and radial (V) components of mean velocities, the corresponding turbulence levels (u & v) and Reynolds shear stress ($\overline{uv}$) were obtained with the single channel anemometer in the manner described by Melling and Whitelaw (1976). Frequency shifting of the laser light was used to detect the direction ambiguity of individual measurements. The optical arrangement of the laser-Doppler anemometer for the velocity measurements have been described in detail by Yu (1991) and is similar to that described by Rojas et al. It operated in forward scatter and made use of a 5mW He-Ne laser, a diffraction grating, a collimating and an imaging lens. The principal characteristics of the optical system are summarised in Table I below.

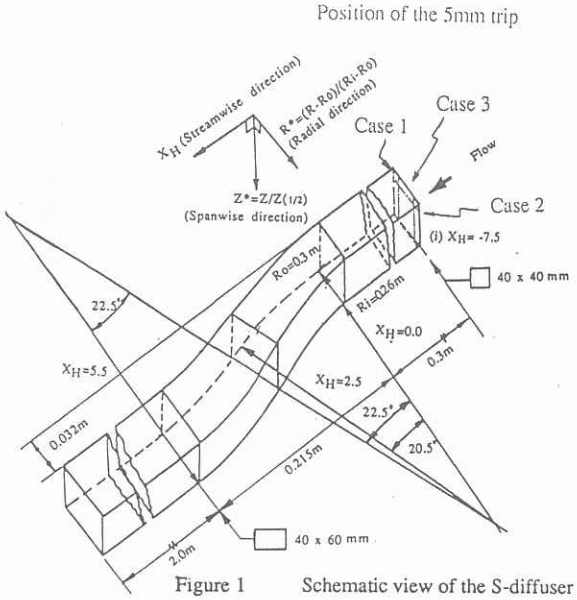

Figure 1 Schematic view of the S-diffuser

The Doppler signals were detected by a photomultipier tube (E.M.I. 9658B) and processed by a digital counter (Imperial College Fluids section model 2, Heitor et al (1984)). A sampling population of 5,000 was obtained for individual measurement to yield the mean and corresponding r.m.s. velocities. An careful appraisal of the experimental uncertainties is given by Yu (1991) and the maximum uncertainties of individual measured mean and corresponding rms quantities do not exceeded 1% and 3% of the inlet bulk velocity. Wall static pressure measurements were obtained by a differential micromanometer.

3. Results and Discussion

Measurements of the streamwise mean components (U) at each measured station were integrated by Simpson's rule to obtain the flow rate which was found to agree with the reading of the flowmeter to within 5%. Flow separation was not detected by wall static pressure measurements and local velocity measurement at each of measuring station for any of the three flows. The results of cases 1 and 2 will be reported first for they are both symmetrical about the plane Z*=0.0 .

3.1 Mean Velocities

a) Cases 1 and 2

The contours of the streamwise mean velocity at the inlet, figures 2a(i) and 3a(i), show that the maximum velocity core with values velocity higher than $0.9U_{max}$, is located close to the inside surface of the first bend with centre around R*=0.7 in case 1 and at R*=0.3 in case 2 due to the presence of the trip upstream. Radial components at this station, figure 2a(ii) and 3a(ii) , are towards the inside wall of the first bend in the three cases responding to the favourable pressure gradient set up by the longutindinal curvature as shown in the static pressure measurements, figure 9 along R*=1.0 line. Large velocities occur close to the bottom side wall in case 1, and indicate a maximum secondary flow velocity of $0.08U_b$ comparing to a measured maxima of $0.09U_b$ in case 2 and is at the centre-region, comparing figure 2a(ii) and 3a(ii).This indicates that the onset of the secondary flow due to curvature is not as early as in case 1.

The contours at the end of the first bend, X_H=2.5, figure 2b(ii) and 3b(ii), show that the maximum velocity core has migrated from R*=0.7 at the inlet to R*=0.5 while in case 2 the maximum velocity region is still at around R*=0.3. The region around R*=0.9 and from Z*=0.0 to -0.5 shows that low velocity fluid has accumulated through the convection of the secondary flow in both cases. This also leads to a negative streamwise velocity gradient, $\partial U/\partial Z^*$ near the plane of symmetry, at around R*=0.9 in case 1 as a consequence of higher secondary flow and the adverse streamwise pressure gradients, also see figure 9. The radial components at this station, figures 2b(ii) and 3b(ii) , have a maximum secondary-flow velocity of $0.14U_b$ and $0.11U_b$ in cases 1 and 2 respectively. The difference is mainly due to the inlet boundary layer thickness along the bottom wall.

TABLE I

Characteristics of the Optical Arrangement

Focal length of imaging lens	200 mm
Half-angle of intersection	8.26^0
Fringe separation (line-pair spacing)	2.04μm
Number of fringes in measuring volume	19
Intersection volume diameter calculated at $1/e^2$ intensity	0.04 mm
Intersection volume length calculated at $1/e^2$ intensity	0.25 mm
Photomultipler pinhole diameter	0.5 mm
Transform constant	2.04(m/sec)/(MHz)
Nominal frequency shift	~ 1MHz

Further downstream at the end of the second bend, X_H=5.5, figures 2c(i) and 3c(i), the region of negative $\partial U/\partial Z^*$ has extended to R*=0.7 and the maximum velocity core migrated further to R*=0.3 in case 1 but no changes in position in case 2. While the changing curvature has caused a complete reversal of direction of the secondary flows in case 2, the radial components in case 1 do not follow this trend, figure 2c(ii), except at the inside wall of the second bend. The region from R*=0.7 to the outside wall still retains some influence of the first bend in which it includes a large vortex rotating in the same sense as in the first bend and occupying almost half of the duct cross-section; the maximum secondary-flow velocity is about $0.12U_b$. Comparing the streamwise mean and radial mean velocity at the exit plane with uniform inlet condition from Rojas et al (1983) and cases 1 and 2 (figure 4) shows that the vortex of case 1 has shrunk to the region around R*=0.9 in Rojas et al, and is absent in case 2. The presence of the vortex of case 1 and Rojas et al also leads to a non-uniform distribution of the streamwise mean contours.

b) Case 3

The contours of the streamwise mean components for case 3 at the inlet, figure 5a(i), show that the trip causes asymmetric streamwise mean velocity distributions about the centre plane of the cross-section, Z*=0.0, with a maximum magnitude at Z*=-0.3. The radial components at this station, figure 5a(ii) are towards the inside surface except at R*=0.1 due to the favourable pressure gradient set up there, the maximum magnitude is relatively lower than the previous two cases and corresponded to a value of $0.04U_b$.

Figure 5b(i) shows that the maximum velocity core in the middle section has migrated towards the outside wall of the bend under the steady strengthening of secondary flow. The region bounded by R*=0.7, 0.9 and Z*=-0.3, -0.8 shows that low velocity fluid has accumulated through the convection of the secondary flow, with stronger secondary circulation in the lower half of the duct. The radial components at this station, figure 5b(ii), confirm this speculation. Higher magnitudes occur below the Z*=0.0 plane with a maximum secondary-flow velocity of $0.12U_b$ at around Z*=-0.3. At the exit of the second bend, figure 5c(i), the maximum velocity core is close to the inside wall of the second bend. The radial components show that two counter rotating vortices have appeared near the outside wall as in case 1 but of lesser strength and size, see figure 5c(ii), and the maximum secondary-flow velocity is $0.09U_b$.

Although the inlet boundary layer, defined by $0.99U_{max}$, is thicker in the upper part of the duct ($0.3D_H$ at the top side wall and $0.175D_H$ at the bottom side wall), the secondary flow is stronger in the lower part. This can be explained by the downward shift of the maximum velocity from the plane of symmetry Z*=0.0 to -0.3 at the inlet, which causes the region above the plane Z*=-0.3 to have a higher effective aspect ratio than in the region below. Thus, it is inappropriate to associate the thicker boundary layer with higher secondary flow in this asymmetric case. This observation confirms the influence of the aspect ratio of the duct on the generation of the secondary flow.The pair of contra-rotating vortices at the exit of second bend in the third case occupies about a quarter of the entire cross-section and is also due to the change of the local sign of $\partial U/\partial Z^*$ gradient to negative in the middle section, figure 5b(i) at R*=0.9 and from Z*=0.2 to -0.7 .

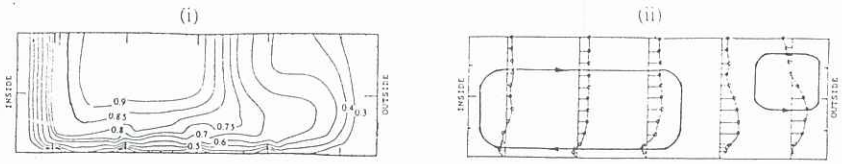

Figure 4 Streamwise mean (U/U_b) velocity contours and Radial mean (V/U_b) velocity profiles at the exit plane, X_H=5.5, with uniform inlet condition (taken from Rojas et al (1983))

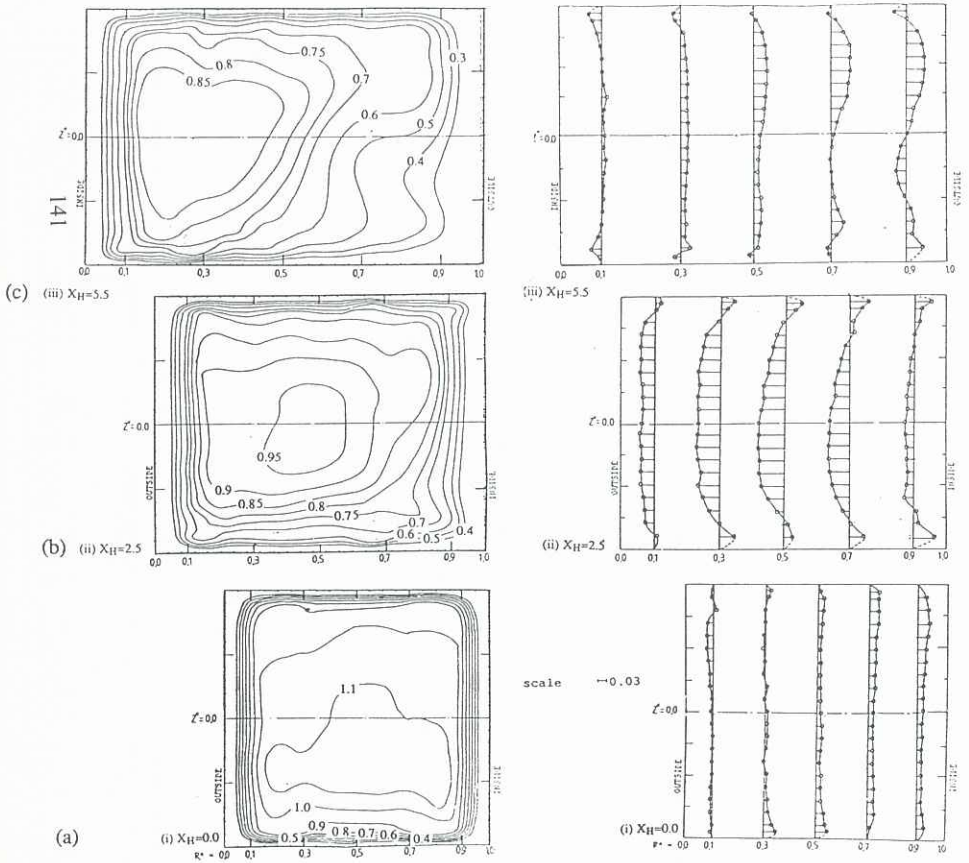

Figure 5 Streamwise mean (U/U_b) velocity contours and Radial mean (V/U_b) velocity profiles at successive stations for case 3

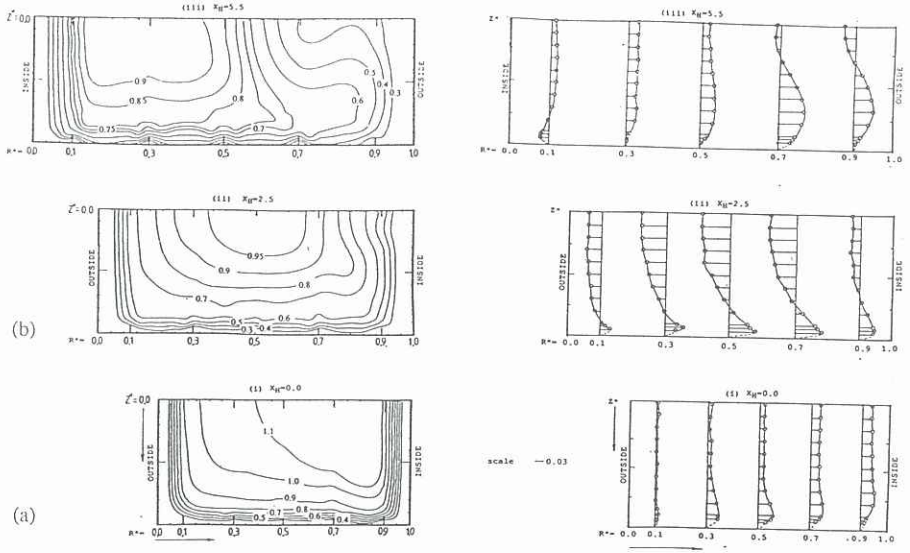

Figure 2 Streamwise mean (U/U_b) velocity contours and Radial mean (V/U_b) velocity profiles at successive stations for case 1

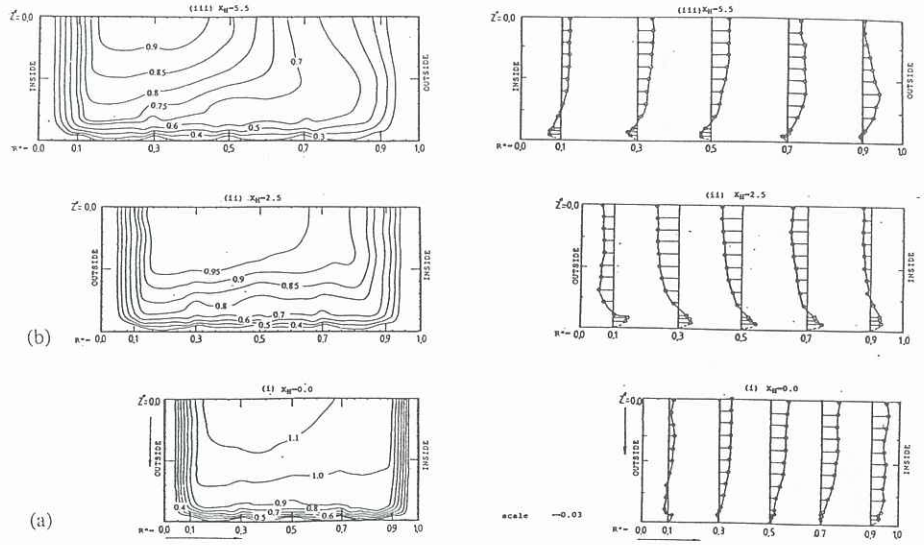

Figure 3 Streamwise mean (U/U_b) velocity contours and Radial mean (V/U_b) velocity profiles at successive stations for case 2

3.2 Reynolds Stresses

Due to limited space, only the results for case 1 at the exit plane are presented, see figures 6, 7 and 8. The presence of the upstream trip in the three cases also increases the magnitude of the streamwise (u) and radial (v) turbulence level as well as the uv shear stress comparing to those of Rojas et al. The streamwise turbulence level has an average measured maximum of $0.15U_b$ and a minimum of $0.04U_b$ compared with $0.09U_b$ and $0.01U_b$ in Rojas et al and the radial turbulence level has a maximum of $0.09U_b$ and a minimum of $0.04U_b$ comparing with $0.06U_b$ and $0.01U_b$ in the duct of Rojas et al. The $\overline{uv}$ components in all the three cases do not exceed $0.005U_b^2$ compared with the maximum value of $0.0015U_b^2$ observed by Rojas et al.

3.3 Wall Static Pressure

The overall pressure recoveries for cases 1, 2 and 3 are 0.187, 0.191 and 0.18 of the velocity head respectively. The development of the wall pressure is also similar, figure 9 (case 1 only) and the pressure gradients, measured on the side walls are antisymmetric about the junction of two bends, X_H=2.5. The total pressure recovery shows a small difference from that of Rojas et al (0.183). Since flow separation did not occur within the diffuser, the changes in the strength of the secondary flow and the loss of or the gain in kinetic energy due to the secondary flow is insufficient to cause a substantial change in the total pressure recovery.

4. Concluding Remarks

The following conclusions can be drawn from the above sections:

1) The location of the maximum velocity core at the inlet of the first bend determines the strength of the secondary flow generated along the bend. In the first case, where the core is located close to the inside surface of the bend, the secondary flow has a maximum of $0.14U_b$. In the second case where the core is located close to the outside surface of the bend, the maximum is $0.11U_b$.

2) In the first case, a larger vortex rotating in the same sense as in the first bend appears near the outside wall of the second bend at the exit and occupies almost half of the duct cross-section with maximum secondary-flow velocity of $0.12U_b$. In the second case, the vortex of case 1 does not appear and this also causes a less non-uniform distribution of the streamwise mean velocity contours with a maximum secondary-flow velocity of $0.08U_b$. The formation of the vortex is mainly due to the changing sign of radial vorticity on entry to the second bend in the first case.

3) The boundary layer on the upper surface at the inlet is 50% thicker than that on the bottom surface, $0.3D_H$ at the top compared with $0.175D_H$ at the bottom and the secondary flow vortex involves cross-stream velocities which are some 25% less. Thus, an increase in thickness of the boundary layer does not augment the secondary flow in this asymmetric case.

4) The turbulence quantities measured in the three cases are higher than those encountered in the cases with symmetric (uniform) inlet condition.

5) The overall pressure recoveries for the three cases are of the same order as that without the influence of an upstream trip, about one fifth of the velocity head.

Acknowledgement

The authors are glad to acknowledge the financial support from the Royal Aerospace Establishment, Ministry of Defence (U.K.) and are grateful to Dr. J. E. Flitcroft for many useful discussions.

References

ANDERSON, B. H., TAYLOR, A. M. K. P., WHITELAW, J. H. and YIANNESKIS, M. (1982)
Developing flow in S-shaped ducts.
Proc. 2nd. Int. Symp. Appl. of L.D.A. to Fluid Mechanic, Lisbon.

BRADSHAW, P.and BANSOD, P. (1972)
The flow in S-shaped ducts.
Aeronautical Quarterly, 23, 131.

BRILEY, W. R. and McDONALD, H. (1984)
Three-dimensional viscous flow with large secondary velocity.
J. Fluid Mech. 144, 47.

GUO, R. W. and SEDDON, J. (1983)
The swirl in an S-duct of typical air intake propulsion.
Aeronautical Quarterly, May., 34.

HEITOR, M. V., LAKER, J., TAYLOR, A. K. M. P. and VAFIDIS, C. (1984)
Instruction manual for the FS "Model 2" Doppler-frequency counter.
Imperial College Fluids Section Report, FS/84/10.

MELLING, A. and WHITELAW, J. H. (1976)
Turbulent flow in a rectangular duct.
J. Fluid Mech., 78, 289.

ROJAS, J., WHITELAW, J. H. and YIANNESKIS, M. (1983)
Flow in sigmoid diffusers of moderate curvature.
Fourth Symposium on Turbulent Shear Flows, Karlsruhe, Germany.

WHITELAW, J. H. and YU, S.C.M. (1992)
Turbulent flow characteristics in an S-shaped diffusing duct.
Proc.6th. Int. Symp. Appl. of L.D.A. to Fluid Mechanics, Lisbon.

YU, S.C.M. (1991)
Flow characteristics in S-shaped diffusing duct.
PhD thesis, University of London.

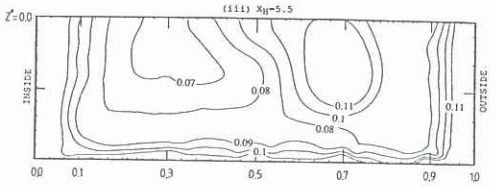

Figure 6 Streamwise turbulence levels (u/U_b) contours at the exit plane, X_H=5.5, for case 1

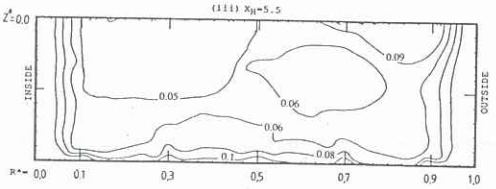

Figure 7 Radial turbulence levels (v/U_b) contours at the exit plane, X_H=5.5, for case 1

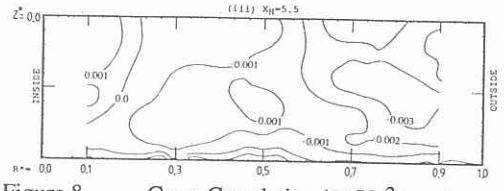

Figure 8 Cross Correlation ($\overline{uv}/U_b^2$) contours at the exit plane, X_H=5.5, for case 1

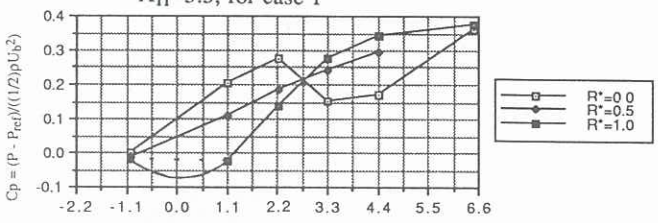

Figure 9 Wall static pressure measurements (Case 1)